Monovalent Cation–Exchanged Natrolites and Their Behavior under Pressure. A Computational Study

ARTICLE *in* THE JOURNAL OF PHYSICAL CHEMISTRY C · SEPTEMBER 2013

Impact Factor: 4.77 · DOI: 10.1021/jp406037c

3 AUTHORS, INCLUDING:

Alena Kremleva
Technische Universität München
16 PUBLICATIONS **139** CITATIONS

SEE PROFILE

Thomas Vogt
University of South Carolina
360 PUBLICATIONS **9,235** CITATIONS

SEE PROFILE

THE JOURNAL OF PHYSICAL CHEMISTRY C

Article

pubs.acs.org/JPCC

Monovalent Cation-Exchanged Natrolites and Their Behavior under Pressure. A Computational Study

Alena Kremleva,[†] Thomas Vogt,[‡] and Notker Rösch[†,§,*]

[†]Department Chemie and Catalysis Research Center, Technische Universität München, 85747 Garching, Germany

[‡]NanoCenter & Department of Chemistry & Biochemistry, University of South Carolina, Columbia, South Carolina 29208, United States

[§]Institute of High Performance Computing, Agency for Science, Technology and Research, 1 Fusionopolis Way, #16-16 Connexis, Singapore 138632, Singapore

Supporting Information

ABSTRACT: Recently natrolite was shown to be an auxetic material that is able to exchange extra-framework Na^+ cations with other mono-, di-, and trivalent cations. Under pressure up to several GPa, these cation-exchanged natrolites undergo superhydration and/or phase transformations in the cation−water arrangement. Using density functional theory we studied in silico the ion exchange in natrolites. First we optimized the structures of Li^+-, Na^+-, K^+-, Rb^+-, and Cs^+-exchanged natrolites at ambient conditions and compared the resulting lattice energies to that of the hypothetical H-form of natrolite. Of all natrolites, the smallest formal exchange energy was found for Na-NAT, in agreement with the natural occurrence of this material. Then we modeled the effect of pressure on Na-, Rb-, and Cs-natrolites, addressing (*i*) the incorporation of water ligands into the zeolite framework, accompanied by an increase in volume; and (*ii*) the changes in the cation−water arrangement within the zeolite pores. The computational models reproduce reasonably well the critical pressure, at which these phenomena occur, and, in the case of Cs-NAT, point toward a cation displacement model for its structural transition under pressure.

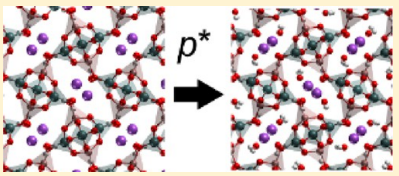

1. INTRODUCTION

Zeolites are aluminosilicates with ordered low-density framework structures that are composed of corner-sharing TO_4-tetrahedra with T = Si or Al.[1,2] As secondary structural units of the framework, one finds windows, cages, channels, and pores of molecular dimension that are able to accommodate cations and water molecules.[1] Zeolites are used in heterogeneous catalysis and for ion exchange in many industrial and environmental applications.[3] These applications are based on the incorporation of aluminum into the framework, which gives rise to charge compensating bridging hydroxyl groups, which, in turn, allow one to tune the acidity of zeolites and exchange protons by low-valent cations.[4,5] Zeolites are also known as "molecular sieves",[2] as they selectively ad- and desorb molecules, primarily due to weak interactions combined with size effects, thus rendering the size of the pores a key characteristic. Zeolite frameworks are rather flexible and respond to temperature and pressure by expansion, contraction, cation exchange, and/or hydration.[6−8] In the present work, we study the cation exchange and pressure-induced structural and compositional changes in naturally occurring natrolite, a small-pore zeolite with an orthorhombic unit cell and the ideal composition $Na_{16}Al_{16}Si_{24}O_{80}\cdot 16H_2O$.[9,10]

Grima et al. provided experimental evidence that natrolite is an auxetic zeolite.[11] As known from classical elastic theory,[12] auxetic materials exhibit negative values of Poisson's ratios; they spatially expand perpendicular to the direction they are stretched. This scenario yields an appealing model for the occurrence of pressure-induced hydration in natrolite.[11] Alderson et al. suggested[13] that auxetic nanoporous materials would allow exquisite control of the pore size and, therefore, facilitate "de-fouling" of membranes, since pore sizes can increase under tensile loads. On the basis of force-field studies, auxetic behavior was predicted for a variety of zeolites, for example, natrolite[14] and laumontite.[15]

Pressure-induced ion exchange and volume expansion of zeolites of the natrolite family were recently reported.[6,8,16,17] Natrolite and related zeolites were not considered earlier for ion exchange due to their rather small pores resulting in steric hindrance; therefore, this type of aluminosilicate frameworks were not well studied. Pressure-induced hydration and subsequent volume expansion of natrolite increases the size and changes the ellipticity of the pores. Thereby, ion exchange and sorption properties of such small-pore zeolites are radically altered.[18−20]

A basic structural motif of natrolite frameworks is corner-sharing rigid polyhedral T_5O_{10} units with T = Al, Si, where the T atoms may be viewed to form roughly a square-pyramid arrangement (Figure 1). Under increasing pressure, these rigid squares undergo an overall rotatory motion (chain rotation angle ψ, Figure 1), resulting in a widening of the nanopores that are defined by 8-ring channels.[6] As a consequence, under

Received: June 19, 2013
Revised: August 13, 2013
Published: September 9, 2013

   dx.doi.org/10.1021/jp406037c | J. Phys. Chem. C 2013, 117, 19020−19030

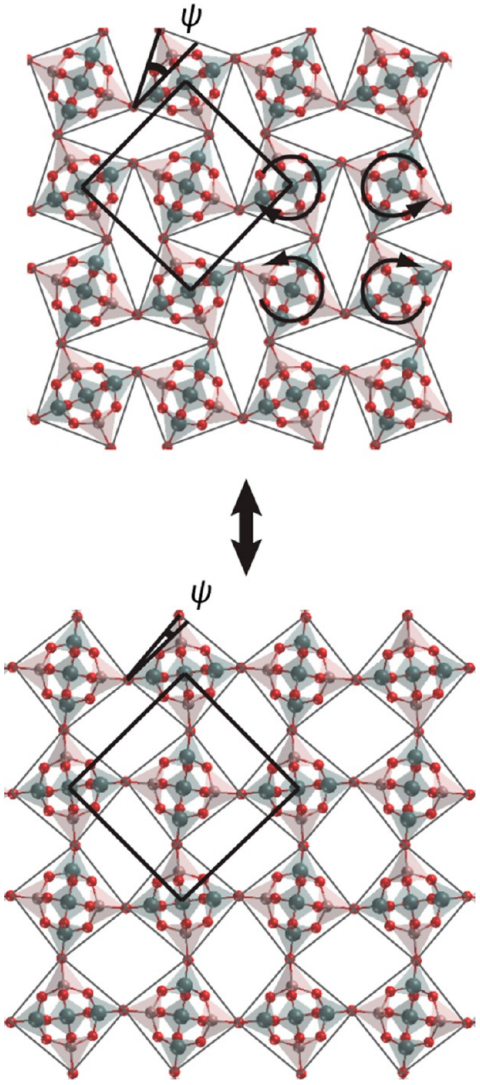

Figure 1. Schematic representation of the channels in natrolites. Cations and aqua ligands are removed for simplicity. ψ is the chain rotation angle, defined as angle between one side of the projected outline of a T_5O_{10} moiety and the side of the square defined by four tops of such moieties, as shown (black solid lines).

pressure more water and larger cations can adsorb into the zeolite pores from the surrounding solution. After releasing the pressure, atomic and molecular species remain trapped inside the cavities with windows that are too small for them to escape ("trap-door" mechanism).[8]

Natrolite frameworks were characterized as either "collapsible" or "non-collapsible", depending on whether the hinges of the T_5O_{10} units co-rotate in the same ("collapsible") or in the opposite ("non-collapsible") directions.[21,22] Such a "rotating squares" mechanism based on rigid tetrahedral units and "soft hinges", leading to pore and volume expansion and concomitant pressure-induced hydration, has been discussed in the literature as one of the ways that auxetic behavior of materials manifests itself at the atomic scale.[23]

Recent experiments demonstrated that one can fully exchange Na^+ ions of the natural natrolite (Na-NAT) by K^+ ions and subsequently exchange K^+ with other mono- and divalent cations under ambient conditions.[18,19] In situ high-pressure cation-exchange experiments were also carried out with K-natrolite to trap aliovalent Eu(III) cations in a natrolite framework.[8] Thus, the poorly studied small-pore substituted natrolites became promising for designing novel storage media, for example, for actinides. To better understand the potential usage of natrolite in radioactive waste management, one has to explore its ion-exchange properties and the response of related natrolites to increasing pressure and temperature. In the present study we develop a computational model of experimentally known substituted natrolites, Li-, Na-, K-, Rb-, and Cs-NAT, with the aim to analyze and rationalize at the atomic scale their behavior under pressure.

2. COMPUTATIONAL DETAILS

We carried out density functional theory (DFT) calculations on periodic slab models using the Vienna Ab Initio Simulation Package (VASP).[24−27] In this code one-electron wave functions are represented by a set of plane waves to solve the Kohn−Sham equations. The core electrons of the atoms are accounted for by the projector-augmented wave approach.[28,29] For the exchange-correlation functional we chose the generalized gradient approximation (GGA) in the form suggested by Perdew, Becke, and Ernzerhof (PBE).[30,31] To examine the effect of van der Waals interactions, we applied the DFT-D approach, where one adds a semiempirical dispersion potential term to the conventional Kohn−Sham expression of the DFT energy.[32] Specifically, we invoked the DFT-D2 method, which describes van der Waals interactions by a simple pairwise force field.[33] The representation in *k*-space was restricted to the Γ-point. Applying a cutoff of 520 eV, we aimed for tight convergence of the plane-wave expansion. In geometry optimizations, the total energy was converged to 10^{-6} eV, and forces acting on ions were required to be less than 10^{-4} eV/pm.

To model the effect of increased pressure on the zeolite structure, we carried out calculations where the shape of the unit cell was varied at constant volume; this strategy also allowed full optimization of the positions of all atoms in the unit cell.[27] The resulting optimized stress tensor, after diagonalization, exhibited very similar diagonal elements. Therefore, the average of these diagonal elements can be taken to represent the negative of the pressure, applied to the system. A similar procedure was used earlier in the literature.[34,35] As the plane-wave basis is not complete with respect to the changes of the shape of the unit cell (and its volume when the bulk is optimized), implied in this procedure, one is interested in estimating the consequences of the resulting Pulay stress. To this end, we optimized exemplary structures with a higher energy cutoff, 800 eV; subsequently, we reoptimized the shape of the unit cell at fixed volume and the standard energy cutoff of 520 eV. We also carried out the reverse procedure; that is, we reoptimized the shape of the unit cell, obtained with a cutoff of 520 eV, using the basis set defined by the cutoff of 800 eV. The resulting stress values of about 0.2 GPa appear to provide an adequate estimate of the pressure uncertainties due to the Pulay stress; for details, see the Supporting Information (SI).

3. RESULTS AND DISCUSSION

3.1. Monovalent Exchanged Natrolites at Normal Conditions: Structures. First we will discuss the results calculated at normal conditions for natrolites of the stoichiometric formula $X_{16}Al_{16}Si_{24}O_{80}{\cdot}16H_2O$ (X-NAT) with monovalent ions X^+ (X = Li, Na, K, Rb, Cs) in the channels.

dx.doi.org/10.1021/jp406037c | J. Phys. Chem. C 2013, 117, 19020−19030

The structures of these X-NAT zeolites have been determined experimentally using X-ray powder diffraction.[18,19] We started the structure optimizations with the corresponding experimental structure, maintaining the orthorhombic shape of the experimentally determined unit cells.

As a reference and for comparison, we also optimized the hypothetical H-form of natrolite, where Na^+ is formally exchanged by H^+. This type of material was experimentally shown to be instable.[36,37] In the optimized structure the protons, attached to frame oxygen centers, were stabilized by hydrogen bonds to aqua ligands. We use this hypothetical structure of H-NAT as reference when discussing the ion-exchange energies (section 3.2).

In Table 1 we compare the optimized unit cell parameters to the corresponding experimental data. The unit cell parameters

Table 1. Unit Cell Vectors (Å) and Unit Cell Volumes (Å^3) as well as Distortion Parameter ψ (deg) for X-NAT (X = H, Li, Na, K, Rb, Cs) Zeolites from Calculations at the PBE and PBE-D2 Levels of Theory[a]

X	method	R_{ion}[b]	a	b	c	V	ψ
H	PBE		17.50	17.89	6.71	2101	30.2
	PBE-D2		16.98	17.54	6.66	1984	32.5
Li	PBE		18.01	18.70	6.58	2216	24.6
	PBE-D2		17.62	18.51	6.53	2130	26.2
	exp[c]	0.90	17.55	18.65	6.47	2118	25.5
Na	PBE		18.45	18.68	6.69	2306	24.4
	PBE-D2		18.25	18.48	6.66	2246	25.3
	exp[d]	1.16	18.33	18.65	6.60	2256	24.0
K	PBE		19.02	20.26	6.58	2536	15.6
	PBE-D2		18.75	20.01	6.54	2454	17.3
	exp[e]	1.52	19.27	19.75	6.48	2466	12.8
Rb	PBE		20.31	20.15	6.62	2709	7.6
	PBE-D2		20.00	19.96	6.58	2627	10.5
	exp[e]	1.66	19.84	20.01	6.54	2596	6.7
Cs	PBE		20.42	20.28	6.66	2758	6.0
	PBE-D2		20.41	20.06	6.60	2702	6.8
	exp[e]	1.81	19.98	20.30	6.56	2661	2.9

[a]Also shown are experimental results and the radii R_{ion} of the ions X^+ (Å). For designation, see Figure 1. [b]Reference 38. [c]Reference 19. [d]Reference 42. [e]Reference 18.

calculated at the GGA level in general overestimate the corresponding experimental values, at most by 0.5 Å (3%) for the unit cell parameters a and b and by 0.1 Å (2%) for vector c. The PBE-D2 method yields mostly shorter unit cell vectors; thus, it reproduces the volume of the unit cell better than the corresponding PBE data. The volume of the unit cell correlates with the radii of the cations inside the zeolite (Figure 2). Figure 2a clearly shows that the volumes optimized at the PBE-D2 level match experimental data, whereas the PBE method somewhat (2−5%) overestimates the volumes of the unit cells, by 50 Å^3 (Na-NAT) to 113 Å^3 (Rb-NAT) Å^3.

Both computational approaches, using PBE and PBE-D2, very well reproduce the decreasing trend of the angles ψ with increasing radius of the alkali counterions (Figure 2b). The large values, ∼25°, of the angles ψ for Li- and Na-NAT agree within ∼1.5° with the corresponding experimental results (Table 1; Figure 2b). Slightly larger deviations are obtained for larger counterions: ∼3° for K- and Cs-NAT at the PBE level and ∼4° for K-, Rb-, and Cs-NAT at the PBE-D2 level. Both

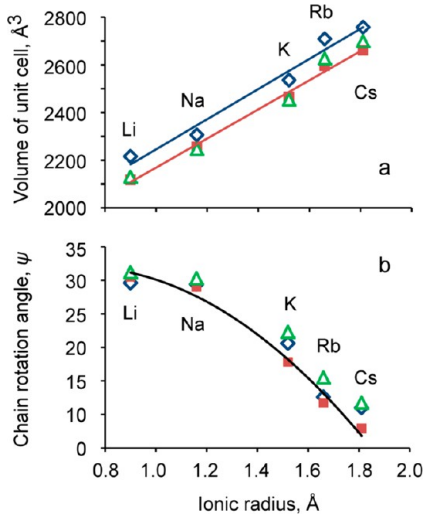

Figure 2. Correlation of (a) the volume (Å^3) and (b) the chain rotation angle ψ (deg) of X-NAT (X = Li, Na, K, Rb, Cs) with the ionic radius (Å) of the ion X^+ in the natrolite framework. Empty diamonds, computational results at the PBE level; empty triangles, computational results at the PBE-D2 level; filled squares, experimental data from refs 18, 19, and 42. Various least-squares fits of the data are shown: (a) red line, linear fit of experimental data, V/Å^3 = 1557.8 + 611.1R_{ion}/Å with R^2 = 0.99; blue line, linear fit of PBE results, V/Å^3 = 1612.4 + 633.1R_{ion}/Å with R^2 = 0.97; (b) quadratic fit to experimental data, ψ/deg = 17.27 + 28.0R_{ion}/Å − 20.2R_{ion}^2/Å^2 with R^2 = 0.99.

computational approaches, PBE and PBE-D2, reproduce the experimental trend in the angles ψ with comparable accuracy.

The extra-framework cations of substituted NAT are coordinated to the oxygen centers of the zeolite framework and to the water molecules present in the channels. Within the zeolite channels, the various cations occupy qualitatively different positions, relative to the axis of the channel along the c direction (Figures 3a, 4a). Using this as a criterion, the structures can be divided into two groups, Li- and Na-NAT (Figure 3) on the one hand, as well as K-, Rb-, and Cs-NAT (Figure 4) on the other hand.

Figure 3 shows the structures for Li- and Na-NAT where the cations are located close to the axis of the channels along the c direction and alternate with water ligands so that each type of species, cations and water molecules, engage in two mutual coordination bonds (Table 2, Figure 3b). In addition to the ion−water interactions, the cations have close contacts to framework O centers. To evaluate such cation−oxygen contacts, we counted distances X−O_{fr} to frame oxygen atoms up to a cutoff value, defined by the longest distance X−O to a water molecule plus a margin of 0.3 Å. For Li-NAT we made an exception and also counted larger distances following the practice of the corresponding experimental study.[19] Table 2 lists the resulting X−O contacts to framework oxygens and aqua ligands. In view of its symmetry, *Fdd*2, the natrolite lattice features only five symmetry-inequivalent framework oxygen centers (Table 2). The labels identifying various oxygen centers are defined in Figure S1 of the SI. Four of the five types of O centers (O1−O4) are part of Al−O−Si moieties, connecting Al and Si tetrahedra; only centers O5 are of Si−O−Si type. The former O centers are more acidic, and the charge balancing extra-framework ions X^+ are expected to coordinate preferably to them. Indeed, in Li- and Na-NAT, one finds exclusively X−O contacts to Al−O−Si oxygen centers, while in K-, Rb-, and

dx.doi.org/10.1021/jp406037c | J. Phys. Chem. C 2013, 117, 19020−19030

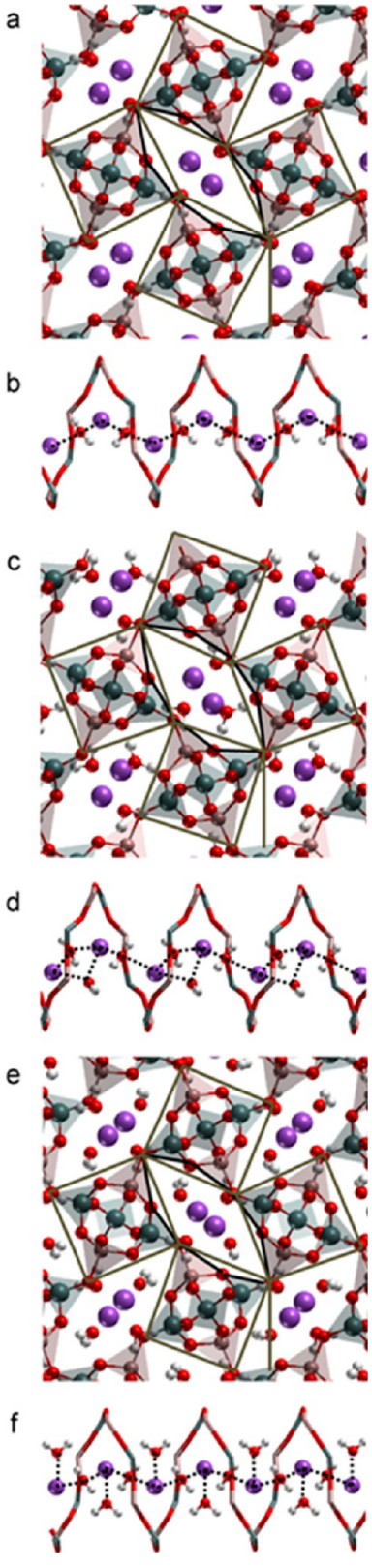

Figure 3. Optimized structures of hydrated forms of Na-NAT under pressure. Na-NAT-16 at ambient conditions: (a) top view; (b) side view of a single channel with a cation−water chain. Na-NAT-24 at 1 GPa: (c) top view; (d) side view of a channel with a cation−water chain. Na-NAT-32 at 1.5 GPa: (e) top view; (f) side view of a channel with a cation−water chain. Dotted lines indicate coordination bonds between cations and aqua ligands in the channels.

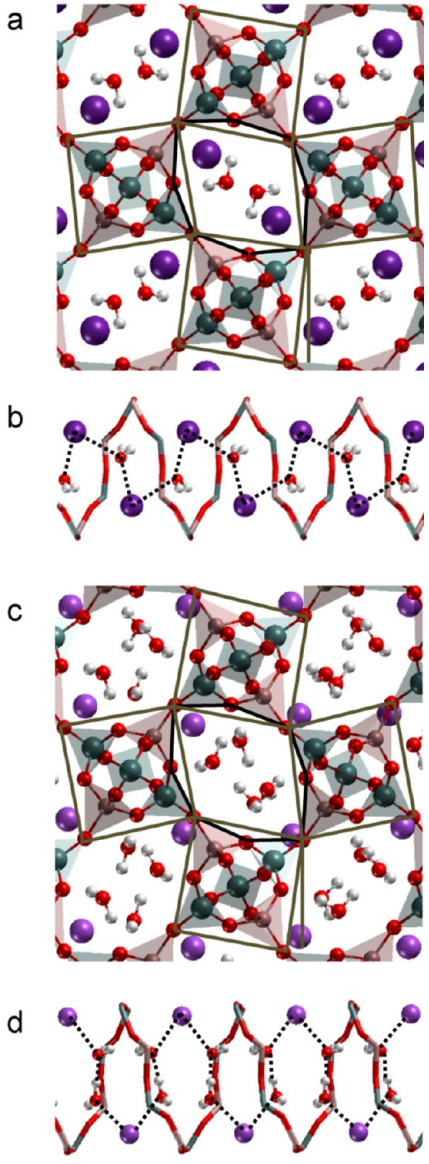

Figure 4. Optimized structures of hydrated forms of Rb-NAT under pressure. Rb-NAT-16 at ambient conditions: (a) top view; (b) side view of a single channel with a cation−water chain. Rb-NAT-32 at 2.5 GPa: (e) top view; (f) side view of a channel with a cation−water chain. Dotted lines indicate coordination bonds between cations and aqua ligands in the channels as well as hydrogen bonds between aqua ligands.

Cs-NAT structures also other contacts occur, between X^+ and Si−O−Si type oxygen centers.

The X−O distances calculated for Na-NAT agree best with the corresponding experimental values. The structure reveals two bonds to water ligands of ∼2.4 Å, which are computationally well reproduced (2.38−2.39 Å for PBE and PBE-D2, Table 2). In addition, the Na^+ ions are coordinated to four framework oxygen centers; the corresponding calculated distances agree with the experiment within 0.06 Å. Using the PBE-D2 method, only two out of six Na−O contacts, those to O2 framework centers, are calculated ∼0.08 Å shorter than the Na−O contacts determined with the PBE functional. The other four Na−O bonds to framework centers as well as to water ligands differ at most by 0.02 Å between the two computational methods, PBE and PBE-D2 (Table 2). Thus, both computa-

dx.doi.org/10.1021/jp406037c | J. Phys. Chem. C 2013, 117, 19020−19030

Table 2. Contacts (Å) of Ions X^+ to O Centers of Aqua Ligands, $X-O_{aq}$, and to O Centers of the Zeolite Frame, X−O*n*, *n* = 1−5, X = Li, Na, K, Rb, and Cs, from Calculations at the PBE and PBE-D2 Levels of Theory

X	method	Occ.[a]	$X-O_{aq}$	X−O1	X−O2	X−O3	X−O4	X−O5
Li	PBE		2.11, 2.40		2.41, 2.83	2.09	2.14	
	PBE-D2		2.18, 2.25		2.23, 2.71	2.10	2.20	
	exp[b]		1.95, 2.32		2.16, 2.64	2.34	2.77	
Na	PBE		2.38, 2.39		2.56, 2.61	2.38	2.37	
	PBE-D2		2.39, 2.39		2.47, 2.54	2.39	2.39	
	exp[c]		2.39, 2.41		2.53, 2.60	2.36	2.40	
K	PBE		2.93, 2.93	2.99		2.90	2.93	2.61
	PBE-D2		2.94, 2.94	2.94		2.84	2.84	2.68
	exp[d] K1	0.59	2.28/2.85[e]	2.82		2.85	2.84	2.87
	exp[d] K2	0.38	3.05/3.01[e]	2.73		3.01	2.91	2.69
Rb	PBE		3.01, 3.01	3.22, 3.40		3.14	3.24	3.27, 3.34
	PBE-D2		3.04, 3.04	3.17, 3.27		3.09	3.15	3.20, 3.27
	exp[d] Rb1	0.50	2.81, 3.21	3.08, 3.39		3.12	3.14	3.15, 3.38
	exp[d] Rb2	0.37	3.31, 3.31	2.92, 3.39	3.36	3.19	3.13	2.92
	exp[d] Rb3	0.06	3.15, 3.15	2.77	3.25, 3.29	3.37	3.34	2.83
Cs	PBE		3.03, 3.22	3.31, 3.31		3.24	3.35	3.30, 3.30
	PBE-D2		3.11, 3.11	3.25, 3.25		3.20	3.27	3.22, 3.22
	exp[d] Cs1	0.49	2.92, 3.31	3.19, 3.26		3.35	3.30	3.25, 3.35
	exp[d] Cs2	0.43	3.26, 3.26	3.06, 3.28	3.48, 3.48	3.33	3.37	3.14, 3.31

[a]When more than one position of the cations was resolved in experiment, the corresponding occupancies are given in addition. [b]Reference 19. [c]Reference 42. [d]Reference 18. [e]Two positions, OW1 and OW2, of aqua ligands resolved in experiment; the first distance given corresponds to the bonds K1−OW1, the second to the K1−OW2 bonds, and similarly for K2 positions.

tional approaches reproduce the experimental structure of Na-NAT rather well.

The structure calculated for Li-NAT does not agree as well with experimental data. In general, the structure is more asymmetric: the two Li−O bonds to the aqua ligands exhibit rather different lengths: 2.11 Å and 2.40 Å (PBE), 2.18 Å and 2.25 Å (PBE-D2), 1.95 Å and 2.32 Å (exp). The $Li-O_{fr}$ contacts, grouped into two shorter and two longer distances, show even larger discrepancies between calculated and experimental results, in particular for the contacts X−O2 (Table 2). However, the range of the $Li-O_{fr}$ distances is well reproduced: 0.74 Å (PBE), 0.61 Å (PBE-D2), and 0.61 Å (exp; Table 2). The ionic radius of Li (0.9 Å)[38] is smaller than that of Na^+ ions (1.16 Å)[38], and the shorter $X-O_{aq}$ distances differ accordingly. However, the lattice parameter *c* (in the direction of the channels holding the ion−water chains) of Li-NAT is only ∼0.1 Å shorter than that of Na-NAT (Table 1). Apparently, this reflects the rigidity of the T_5O_{10} blocks. Thus, Li^+ ions bind more strongly to one of the neighboring water ligands; formally, the cations slightly move toward one of their neighboring ligands (Figure 3b), creating an asymmetric bonding arrangement also to the framework oxygen centers (Table 2). The experimental structure also shows this asymmetric positioning of the Li^+ ions.[19]

In K-, Rb-, and Cs-NAT, ions and water molecules are arranged inside the channels in a way that differs from that of Li- and Na-NAT (Figures 3, 4). The water ligands are located closer to the channel axis than the cations; Figure 4a illustrates this for the Rb-NAT structure. In the channels, a zigzag chain is formed, with the cations at corner positions, bridged by O centers of water ligands (Figure 4b). K^+ exhibits four contacts to the framework oxygen centers, just as Na^+, whereas Rb^+ and Cs^+ form six such contacts. Recent experiments resolved at least two positions for K^+, Rb^+, and Cs^+ in the zeolite frameworks.[20] Two water positions were also identified in the K-NAT structure.[20] An earlier experiment[18] on Rb-NAT found three positions for the cations and two positions for aqua ligands. Although the occupancy of the corresponding positions of the cations is given, the most probable structures of the two experiments do not match; see Table 2 of ref 18 and the tables in the Supporting Information of ref 20. These latter, more recent results are considered to present improved structural models. However, this diversity of the results may point to less strong anchoring of cations inside the zeolite framework or even a dynamical behavior, and calls for neutron powder diffraction experiments.

In silico we were able to determine only a single position for each cation. In K-NAT we found an isomer where the K^+ position corresponds to the one experimentally labeled as K2 (Table 2). The optimized distances $K-O_{aq}$ of 2.93−2.94 Å agree with all the $K-O_{aq}$ distances of the experiment, except for the shortest one, 2.28 Å, which corresponds to the bond between K1 and the O center of one of the water ligands (Table 2). In the optimized K-NAT structure, the four contacts $K-O_{fr}$ to the framework are dispersed by 0.26−0.38 Å, which was observed experimentally only in the case of K2, 0.32 Å, while the K−O contacts to the framework in the case of structure K1 of K-NAT vary at most by 0.05 Å (Table 2). Therefore, we are convinced that the optimized structure of K-NAT corresponds to the second isomer with the K2 positions. The experimentally determined occupancies are 0.59 for K1 and 0.38 for K2.[18] Thus, the calculations reproduced the less probable isomer of K-NAT.[18] As for the water oxygen positions, both had very similar occupancies, with 0.41 and 0.46.[18] They also exhibit rather similar coordination bonds to K^+ ions, 3.05 Å and 3.01 Å.

In the optimized structure of Rb-NAT (Figure 4), the Rb^+ ions have two bonds to aqua ligands at ∼3 Å (Table 2) and six contacts to framework oxygen centers with distances in the ranges 3.14−3.40 Å (PBE) and 3.09−3.27 Å (PBE-D2). Either structure, obtained with the PBE or the PBE-D2 approach, agrees rather well with the experimentally determined positions

dx.doi.org/10.1021/jp406037c | J. Phys. Chem. C 2013, 117, 19020−19030

of the cations Rb1 (Table 2).[18] The positions of Rb1 had the highest occupancy with 0.5, compared to 0.37 for Rb2 and 0.06 for Rb3.[18] The six distances Rb1−O_{fr} range from 3.08 Å to 3.39 Å. These values agree very well with the calculated results; differences are at most 0.14 (0.12) Å using the PBE (PBE-D2) functional. The locations of Rb2 and Rb3 have additional contacts to O2 framework oxygen that are not found in the calculated structures.

The structure of Cs-NAT exhibits a similar cation−water arrangement in natrolite channels as Rb-NAT. Experimentally two positions for the Cs^+ ions with rather similar occupancies were found in Cs-NAT, Cs1 (0.49) and Cs2 (0.43).[18] The main difference between Cs1 and Cs2 is the contact to the O2 framework centers. Structure Cs1 does not exhibit any bonds to O2 centers, while Cs2 does coordinate to them. However, these Cs−O bonds are comparatively long, 3.48 Å. The structure of Cs-NAT, optimized with the PBE functional, agrees with the positions Cs1, while the structure optimized on the PBE-D2 level agrees better with Cs2. First of all, the PBE structure exhibits two different Cs−O_{aq} bonds, just as the experimental position Cs2; in contrast, the PBE-D2 structure shows two identical coordination bonds to water ligands, as in the experimental position Cs1 (Table 2). The Cs-NAT structure optimized at the PBE level and the experimental result Cs1 also show very similar distances Cs−O1 and Cs−O5. In turn, the PBE-D2 optimized structure features two rather long contacts Cs−O2, ∼3.5 Å, in agreement with the experimental position Cs2. Thus, PBE and PBE-D2 levels reproduce different experimental isomers. Yet, in both isomers Cs positions have almost the same occupancies and, hence, are equally probable. To compare the two structures, we carried out, using the PBE-D2 approach, a single-point calculation of the structure optimized with the PBE functional and vice versa. The resulting energy differences were just 2 kJ mol^{-1} (PBE) and 1.5 kJ mol^{-1} (PBE-D2) per Cs^+ ion; for details, see the SI. This reflects the fact that the potential energy surface is rather flat between these two structures.

Comparing the overall results obtained with both approaches, PBE and PBE-D2, one notes that, in general, the unit cell parameters, the chain rotation angle ψ, as well as X−O bonds to the water ligands and to the framework oxygen centers are calculated with roughly the same accuracy. Both sets of structures compare well with the experiment. In the cases of isomers, for K-NAT and Rb-NAT, both methods agree on the same preferred isomer, but for Cs-NAT the preference differs, depending on the computational approach (see above). Thus, for structures of the type of zeolites studied, at ambient conditions, the empirical D2 corrections to the PBE functional are of minor importance.

3.2. Monovalent Exchanged Natrolites at Normal Conditions: Energetics. We will discuss three types of energies to characterize the energetics of the X-NAT systems: (*i*) the energy $\Delta E_{X\text{-}aq}$ of a single ion−water interaction inside the zeolite framework; (*ii*) the strain energy ΔE_{str} of the zeolite framework; (*iii*) the ion-exchange energy ΔE_{ex} of X-NAT relative to the hypothetical protonated H-form of natrolite.

3.2.1. Ion−Water Interaction in the Zeolite Framework. To estimate the ion−water interaction energy ΔE_{int} in the zeolite framework, we formally separate the system into two parts: (1) the zeolite with the cations in the channels, but without water, and (2) the aqua ligands in the same arrangement as inside the zeolite channels. We carried out single-point (sp) calculations of these two subsystems, where the positions of the atoms are kept fixed as in the optimized structures of X-NAT with water in the channels. Then the interaction energy ΔE_{int} between the cations in the zeolite framework and the aqua ligands is the energy change during the following formal reaction:

$$\text{X-NAT-16H}_2\text{O(opt)} \rightarrow \text{X-NAT(sp)} + 16\text{H}_2\text{O(sp)} \quad (1)$$

This energy corresponds to 16 cations interacting with 16 water molecules inside the zeolite frame. As each cation exhibits two bonds to water ligands, a single ion−water interaction will be $\Delta E_{X\text{-}aq} = \Delta E_{int}/32$. One expects that these energies will vary with the ionic radius of X^+ and decrease gradually with increasing radius of X^+. Indeed, such a correlation exists for the average ion−water interaction energy $\Delta E_{X,sol}$ in aqueous solution (Table 3) if one approximates the latter energy by the experimental hydration enthalpy ΔH_{sol} of the cation X^+ (taken from ref 39) divided by the average coordination number (taken from ref 40). For the calculated $\Delta E_{X\text{-}aq}$ values, such a trend holds only approximately as the interaction energy of K^+ and water is even lower than that of Cs^+ and water, using both computational approaches (Table 3).

Table 3. Energy Characteristics (kJ mol^{-1}) per Ion[a]

energy		method	Li	Na	K	Rb	Cs
ion−water	$\Delta E_{X\text{-}aq}$	PBE	57	55	35	41	36
		PBE-D2	75	72	43	53	49
	$\Delta E_{X,sol}$	exp[c]	87	68	46	37	33
strain	ΔE_{str}	PBE	10	0[d]	45	77	83
		PBE-D2	8	0[d]	45	87	103
ion exch.	$\Delta E_{ex}(H^+)$	PBE	126	105	121	112	110
		PBE-D2	94	69	102	73	76
	$\Delta E_{ex}(Na^+)$	PBE	21		16	7	5
		PBE-D2	25		33	4	7

[a]Estimated from calculations on X-NAT (X = Li, Na, K, Rb, Cs) at the PBE and PBE-D2 levels of theory. $\Delta E_{X\text{-}aq}$, ion−water interaction in the zeolite framework; $\Delta E_{X,sol}$, the corresponding ion−water interaction in solution (enthalpy per coordination number of the cation); ΔE_{str}, strain energy of the Na-NAT framework when X^+ is replaced by Na^+; $\Delta E_{ex}(H^+)$, exchange energy of proton in H-NAT by X^+; $\Delta E_{ex}(Na^+)$, energy of Na^+ ion exchange by X^+. [b]For details, see section 3.2. [c]Solvation energies for cations are taken from ref 39; coordination numbers are from ref 40. [d]With reference to Na-NAT.

The calculated energies $\Delta E_{X\text{-}aq}$ fall into two ranges (Table 3): 55−57 kJ mol^{-1} (PBE) or 72−75 kJ mol^{-1} (PBE-D2) for Li-NAT and Na-NAT, on the one hand, and 35−41 kJ mol^{-1} (PBE) or 43−53 kJ mol^{-1} (PBE-D2) for K-, Rb-, Cs-NAT, on the other hand. Water ligands in Li-NAT and Na-NAT interact more strongly with the nonframework cations than water ligands in K-NAT, Rb-NAT, and Cs-NAT. These energy trends roughly scale with the calculated distances, X−O_{aq} (Table 2). We obtained 2.11−2.40 (PBE) and 2.18−2.39 (PBE-D2) Å for Li−O_{aq} and Na−O_{aq}, while in K-NAT, Rb-NAT, and Cs-NAT the cation−water bonds were determined in the range 2.93−3.22 (PBE) and 2.94−3.11 (PBE-D2) Å. These two groups of natrolites are also characterized by different types of ion−water arrangement in the channels (Figures 3b, 4b). From the calculated energies $\Delta E_{X\text{-}aq}$, one concludes that the ion−water chains in Li-NAT and Na-NAT are characterized by stronger binding than in the second group, K-, Rb-, and Cs-NAT. Thus ion−water chains in Li-NAT and Na-NAT are expected to be more rigid, implying better defined ion positions. Recall, that

dx.doi.org/10.1021/jp406037c | J. Phys. Chem. C 2013, 117, 19020−19030

these latter natrolites were experimentally characterized by only one isomer, whereas in K-, Rb-, and Cs-NAT various positions of the cations were found.

As mentioned above, the value $\Delta E_{X\text{-}aq}$ determined for K-NAT is lower than expected from the rough trend observed for the other X-NAT systems. Recall that the average $K-O_{aq}$ distances in the zeolite framework and the corresponding coordination numbers (CN) also differ from their values in solution. The coordination numbers of the other cations, Li^+, Na^+, Rb^+, and Cs^+, are the same in the zeolite framework and in solution, and the corresponding distances $X-O_{aq}$ are similar for cations in zeolites and in solution; the differences are less than 0.1 Å, see ref 40. Therefore, we refrain from discussing them here in detail. In K-NAT, the coordination number of K^+ is 6, while in solution 7 was found to be preferred.[40] The average distance $K-O_{aq}$ in zeolite is 2.93−2.94 Å, which is 0.15−0.2 Å longer than the average $K-O_{aq}$ in solution (2.72 Å for CN = 6, 2.80 Å for CN = 7).[40] The longer $K-O_{aq}$ value suggests a weaker K−water interaction, in agreement with the rather low value $\Delta E_{X\text{-}aq}$. In addition, K^+ in the zeolite is undercoordinated, compared to K^+ in aqueous solution. In the experiment, the water content of K-NAT increases upon soaking in water, from 14 to 21 H_2O per unit cell,[18] resulting on average in CN = 7 of K^+. For the optimized structure of K-NAT with 24 water H_2O per unit cell, we calculated $\Delta E_{X\text{-}aq}$ = 41 kJ mol^{-1} per single water ligand (PBE). This result agrees better with the expected trend of decreasing values of $\Delta E_{X\text{-}aq}$ with increasing ionic radius.

3.2.2. Strain Energy of the Zeolite Framework. To estimate the strain energy ΔE_{str} of the zeolite framework due to ion exchange, we carried out single-point calculations on model structures where the monovalent ion X^+ was substituted by Na^+ and the water ligands were removed from all zeolite frameworks. Recall that only Na-NAT occurs in nature. In the following, we focus on the PBE results for the energy values ΔE_{str} per ion; the strain energies do not vary much when the D2 approach is used (Table 3). The estimated values of the strain energy increase with increasing *changes* of the volume.

The strain energy is needed to open the channels of the framework, to increase the T−O−T angle, and to decrease the chain rotation angle ψ. With only 10 kJ mol^{-1} per cation, the strain associated with Li^+ exchange was estimated to be the smallest. In fact, the chain rotation angle ψ remains almost unchanged when Na^+ is substituted by Li^+ (Table 1). To widen the zeolite channels by substituting larger K^+ ions for the Na^+ ions, 45 kJ mol^{-1} are required and the chain rotation angle ψ decreases by ∼9°. The changes of the zeolite frameworks of Rb-NAT and Cs-NAT relative to Na-NAT are more noticeable, along with strain energies of ∼80 kJ mol^{-1} (Table 3). However, the strain of Rb-NAT or Cs-NAT relative to K-NAT is notably lower, 17 and 22 kJ mol^{-1} per ion, respectively (calculated in the same manner as for Na-NAT, but relative to K-NAT).

X-NAT natrolites with exchanged monovalent ions X = Li^+, Rb^+, and Cs^+ are synthesized using K-NAT. Apparently, the changes in the lattice are too large for Na^+ to be exchanged directly by Rb^+ or Cs^+. The exchange of K^+ by Li^+ is thermodynamically preferred, as the exchange energy of Li^+, relative to K-NAT, estimated in the following section, is lower than that relative to Na-NAT.

3.2.3. Ion-Exchange Energies. Finally we estimate the energy ΔE_{ex} per exchanged proton in the hypothetical H-form of natrolite by monovalent cations. For this analysis we use the energy change due to the following formal reaction where the exchanged cations are solvated in an aqueous medium:

$$\text{H-NAT} + 16X^+(\text{sol.}) \rightarrow \text{X-NAT} + 16H^+(\text{sol.}) \quad (2)$$

The energies of the solvated ions X^+ were estimated from those of the corresponding atoms X using experimental values for ionization potentials[41] and solvation enthalpies[39] $\Delta H_{sol}(X^+)$ of the cations:

$$X \rightarrow X^+(\text{sol.}) + e^- \quad (3)$$

The resulting energies, $\Delta E_{ex}(H^+)$, per exchange of one ion, are given in Table 3. All reaction energies of ion exchange, eq 2, are endothermic. This result points to the relative stability of the H-form of natrolite. However, experiments showed that this material is not stable.[36] Our way of estimating $\Delta E_{ex}(H^+)$ is somewhat approximate, of course. We used H-NAT only as a common reference for the other ion-exchanged natrolites X-NAT. The exchange energy of Na-NAT is least endothermic relative to the H-form, 105 kJ mol^{-1} using the PBE functional and 69 kJ mol^{-1} using the PBE-D2 method (Table 3). By this criterion, the naturally occurring Na-NAT is the most stable material of all alkali exchanged natrolites studied. The exchange of a proton of the hypothetical H-form of natrolite by Rb^+ or Cs^+ requires 112 and 110 kJ mol^{-1} (PBE), respectively; the corresponding values determined with the PBE-D2 method are 73 or 76 kJ mol^{-1}. The exchange by Li^+ or K^+ is even more endothermic than that by Rb^+ or Cs^+, 126 and 121 kJ mol^{-1} (PBE; 94 and 102 kJ mol^{-1} with the PBE-D2 method).

The relative stabilities among the X-NAT systems, X = alkali, are easily recognized, when one references the ion exchange relative to the most stable form, Na-NAT; see the energies $\Delta E_{ex}(Na^+)$ in Table 3. The exchange of Na^+ by K^+ is estimated to be 16 kJ mol^{-1} per ion (PBE; PBE-D2: 33 kJ mol^{-1}). Interestingly, the substitution of Na^+ by Rb^+ or Cs^+ requires at most 7 kJ mol^{-1}. However, the Rb and Cs forms of natrolite are experimentally obtained from K-NAT. One should keep in mind that the zeolite channels need to be opened first to allow for the exchange by larger cations. Thus, the strain energy of the framework has to be taken into account because it represents the energy required for opening the channels. This aspect may play the role of a barrier in the exchange of cations. The strain energy of the framework, 45 kJ mol^{-1}, for the exchange of Na^+ by K^+ is the lowest one among the larger cations, K^+, Rb^+, and Cs^+ (Table 3). Thus, starting from Na-NAT, this exchange seems to be the most feasible one, as it has the lowest energy requirement.

This argument does not hold for Li^+, though. The corresponding strain energy is the lowest one, near 10 kJ mol^{-1}, while the exchange energy is similar to that of K^+. Thus, one should expect that the exchange of Na^+ by Li^+ may even be more feasible than the exchange by K^+. In fact, direct exchange of Na^+ by Li^+ has been observed.[42] However, if one aims for a general strategy for subsequent exchange of extra-framework cations, K-NAT serves better than Li-NAT, as it already has widened channels to host larger cations. Furthermore, exchange by larger ions, replacing K^+ by Rb^+ or Cs^+, is exothermic (Table 3).

3.3. Pressure-Induced Hydration and Phase Transition in Natrolites. Thus far, we have discussed the properties of natrolites X-NAT at ambient conditions. Recent experimental studies of this class of materials revealed interesting properties under pressure, even for moderately high values, up to 5 GPa.[6−8,16,17] In particular, Na-NAT exhibits inverse-pressure

effects, that is, volume expansion.[6] Under pressure the channels widen, ultimately increasing the volume while additional water is inserted in the natrolite channels; this is referred to as superhydration.[6,7] Similar effects have been observed for Rb-NAT.[20] In Cs-NAT the cations and ligands adopt a new structural arrangement inside the channels under pressure.[20] Finally, K-NAT under pressure reveals both the insertion of water and the emergence of a new structure of the cation−water arrangement.[20]

We examined computationally the behavior of Na-, Rb-, and Cs-NAT under pressure. In the following we will discuss pressure-induced superhydration of Na-NAT (which occurs in two steps), one-step hydration of Rb-NAT, and the phase transformation of Cs-NAT. The behavior of K-NAT under pressure is more complicated[20] than that of the other X-NAT materials explored in the present work. It involves superhydration and a complex series of structural transformations. We shall describe these investigations in detail elsewhere together with the incorporation of Eu(III) into K-NAT.[8]

3.3.1. Two-Step Superhydration of Na-NAT under Pressure. Experiments showed that water insertion in Na-NAT under pressure (superhydration) occurs in two steps. The first stage is accompanied by a volume increase, while the volume decreases in the second.[7] The critical pressure values, at which additional water is inserted, are not precisely known. Measurements were carried out at 0.8 GPa (16 H_2O per unit cell), at 1 GPa (24 H_2O), and at 1.5 GPa (32 H_2O).[6,7]

We modeled three structures of Na-NAT: Na-NAT-16—with 16 H_2O in the unit cell with a 1:1 ratio of Na^+ and H_2O ligands; Na-NAT-24—with 24 H_2O per unit cell, which corresponds to a 2:3 ratio Na/H_2O; and Na-NAT-32—the superhydrated form, with 32 H_2O per unit cell with two aqua ligands per Na^+ ion. We varied the pressure from 0 to 2 GPa for the structures Na-NAT-16 and Na-NAT-24, and from 1.5 to 5 GPa for Na-NAT-32. Figure 3 shows the optimized structures of Na-NAT-16 at ambient conditions: Na-NAT-24 at 1 GPa and Na-NAT-32 at 1.5 GPa. As described earlier, the cations of Na-NAT-16 are bonded in the channels to water ligands and form chains where each aqua ligand is oriented in such a way that it is coordinated to two Na^+ ions (Figure 3b). In Na-NAT-24 every second pair of neighboring cations is now connected to two water ligands instead of one (Figure 3c,d). When the number of H_2O ligands increases from 24 to 32 in the unit cell, all apparent space is filled up (Figure 3e,f). The cations of Na-NAT-32 are bonded to two ligands in a chain as in Na-NAT-16, but in addition every cation now coordinates one extra water molecule in the first coordination shell, no longer shared with other Na^+ ions (Figure 3f). Comparative inspection of Figure 3 of this work and Figure 3 of ref 7 (exp) reveals a nice agreement. Thus, our model correctly represents the structures of Na-NAT at different states of superhydration.

Figure 5a,b displays the $p-V$ diagrams resulting from calculations with either method, PBE and PBE-D2, together with the experimental data. As expected, the PBE results overestimate the volume at all values of the pressure studied. In general, at a given pressure, the values of the unit cell volume obtained using the PBE functional lie ~50 $Å^3$ above the experimental curve (Figure 5a). The PBE-D2 results for Na-NAT-16 agree very well with experiment (Figure 5b). However, the volume of Na-NAT-24 is underestimated with the PBE-D2 method, as well as the volume of Na-NAT-32 at pressure values between 1.5 and 5 GPa. We also estimated the bulk modulus of Na-NAT-16 and superhydrated Na-NAT-32,

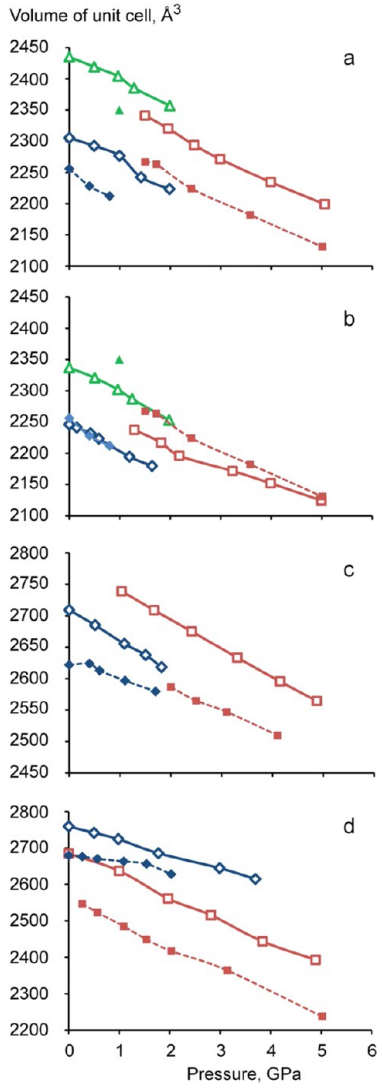

Figure 5. $p-V$ diagrams from PBE (a, c, d) and PBE-D2 (b) calculations (empty symbols, solid lines) for (a) Na-NAT, (b) Na-NAT, (c) Rb-NAT, and (d) Cs-NAT. Experimental data from ref 20. are also shown (solid symbols, dashed lines). Diamonds represent data for X-NAT-16, triangles for Na-NAT-24, and squares for X-NAT-32, except for Cs-NAT-16 where squares represent data for the second isomer.

applying a previously used method.[43] The corresponding experimental values,[6] 53 GPa (Na-NAT-16) and 49 GPa (Na-NAT-32) are notably overestimated at both levels of theory: 60 and 57 GPa (PBE), respectively, as well as 58 and 73 GPa (PBE-D2). The experimentally observed reduction of the bulk modulus $k = -V\cdot\partial p/\partial V$ with increasing pressure is reproduced with the PBE functional but not with the PBE-D2 method. This is an apparent limitation of the empirical D2 correction. Therefore, we restrict the remainder of this section to results based on the PBE functional, which, as expected, slightly overestimates the experimental values as a consequence of the overestimated volume of the unit cell.

To estimate the pressure at which superhydration occurs, one needs to determine the pressure p^*, at which the enthalpy change $\Delta H(p)$ of the following reaction is zero:

$$\text{Na-NAT-}n\text{H}_2\text{O} + m\text{H}_2\text{O} \rightarrow \text{Na-NAT-}(n+m)\text{H}_2\text{O} \quad (4)$$

dx.doi.org/10.1021/jp406037c | J. Phys. Chem. C 2013, 117, 19020−19030

Here n = 16 or 24 and m = 8. Recall that one obtains the enthalpy H from the internal energy U via $H(p) = U(p) + pV$. To determine the enthalpy of water, we optimized the structure of a unit cell with 16 H_2O molecules, at pressure values up to 2.5 GPa. As a result, the enthalpy of either side of eq 4 is approximated by a fit linear in p of the corresponding $H(p)$ values; for details see the SI.

The resulting critical pressure values p^*, for which $\Delta H(p^*) = 0$, are listed in Table 4. We estimated the critical pressure of the

Table 4. Critical Pressure p^* (GPa) for Superhydration, x $H_2O \rightarrow y$ H_2O, in Na-NAT and Rb-NAT, as well as the Phase Transition in Cs-NAT

	Na-NAT		Rb-NAT	Cs-NAT
$x \rightarrow y$	16 → 24	24 → 32	16 → 32	16 → 16
calc[a]	2.3 ± 0.6	2.4 ± 0.4	2.7 ± 0.4	1.0 ± 0.7
exp[b]	0.8−1	1−1.5	1.7−2	0.3−1.5

[a]Results of PBE calculations. [b]Reference 20.

16 → 24 transformation at 2.3 ± 0.6 GPa and that of 24 → 32 at 2.4 ± 0.4 GPa. The method for determining the critical pressure and its uncertainties is described in the SI. The computational values for p^* are very close for the two subsequent hydration steps of Na-NAT. These results qualitatively reproduce the experimental trend, with transformations at 0.8−1 GPa and 1−1.5 GPa, respectively. The values estimated computationally are about 1 GPa larger than the corresponding experimental ones. Taking into account the approximate way of estimating the critical pressure, the lack of entropic contributions and temperature effects, as well as the overestimation of the volume due to the PBE exchange-correlation functional, the agreement with the experiment is acceptable.

To appreciate this, recall earlier computational work that addressed the phase transition in laumontite under pressure using lattice dynamics based on an empirical force field.[15] The structure of laumontite was optimized at various pressures, for 0−15 GPa. The critical pressure was predicted at ∼3.5 GPa,[15] while the corresponding experimental value had been estimated at 1.2 GPa.[6]

3.3.2. Rb-NAT Superhydration under Pressure. Rb-NAT incorporates 16 H_2O into the unit cell at a pressure between 1.7 and 2 GPa. At the lower pressure, 16 H_2O had been experimentally found in the unit cell, while 32 H_2O per unit cell were determined at higher pressures.[20] We modeled the behavior of Rb-NAT-16 at pressure values up to 2 GPa, while we examined Rb-NAT-32 in the pressure range 1−5 GPa. Figure 4 shows the optimized structures of Rb-NAT-16 at normal conditions and of Rb-NAT-32 at p = 2.5 GPa. In Rb-NAT-32 the additional water molecules incorporated under pressure locate near the axes of the channels, while the Rb^+ ions move to the edges of the channels (Figure 4a,c). In the experiment, similar behavior was observed.[20] In Rb-NAT-16 at normal conditions, zigzag chains of alternating water molecules and cations are present (Figure 4b). Additional water molecules inserted into the channels alter the cation−water bonds of Rb-NAT-16. As a result, a Rb^+ cation is coordinatively bonded to a water ligand, which in turn has a rather short H-bond of ∼1.7 Å to the next aqua ligand, that then coordinates with the next Rb^+ ion (Figure 4d). In addition, each Rb^+ ion engages in one more coordination to a water molecule located in a neighboring channel, ∼3.1 Å. In the experiment, rather short distances, ∼2.6 Å, were found between the oxygen centers of two neighboring water ligands; this finding hints at H-bonds between these water ligands and calls for further investigations using neutron powder diffraction. Our computational results confirm the experimentally determined structure of Rb-NAT-32 at higher pressure.

Figure 5c compares experimental and calculated $p-V$ diagrams for Rb-NAT. At a critical pressure near ∼2 GPa, when additional water is inserted into the unit cell, the volume of the unit cell increases in the experiment by only ∼10 $Å^3$, while the computational values differ by 50−100 $Å^3$ in this pressure region. We estimate the critical pressure p^* for the change in hydration to be 2.7 ± 0.4 GPa, proceeding in the same manner as for Na-NAT (for details, see the SI). As in the previous case, the calculated value of p^* overestimates the experimental value of ∼2 GPa by ∼1 GPa. Again, the experimental trend is confirmed: the pressure-induced hydration of Rb-NAT occurs at a higher pressure than that of Na-NAT (Table 4).

3.3.3. Cs-NAT Phase Transition under Pressure. Cs-NAT does not exhibit superhydration under pressure; rather, it undergoes a phase transition.[20] The two phases differ by the positions of the ions and the aqua ligands in the channels and coexist in the pressure range between 0.3 and 1.5 GPa.[20] In the first phase at low pressure, cations and water ligands are arranged as in the structure of Rb-NAT; cf. Figure 4a and Figure 6a, left panel. In contrast, the new phase at higher

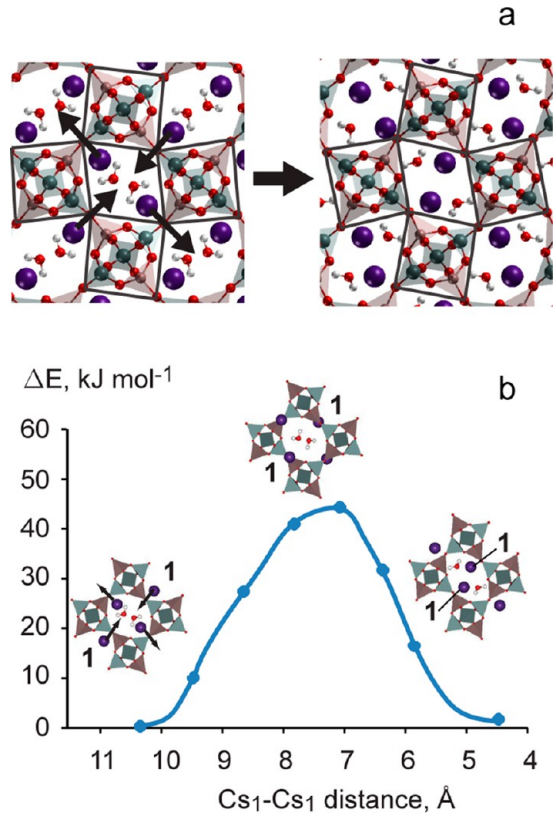

Figure 6. Phase transition of Cs-NAT-16 under pressure. (a) Suggested structure change from low (left) to high pressure (right); arrows represent the directions of the motion of cations. (b) Corresponding energy variation ΔE per ion from constrained optimizations along a path that connects the two structures shown in (a), at fixed pressure, 1 GPa.

dx.doi.org/10.1021/jp406037c | J. Phys. Chem. C 2013, 117, 19020−19030

pressure has a smaller volume and a Cs^+-H_2O arrangement similar to that found in Na-NAT; the Cs^+ ions are determined to be close to the axis of the channels (Figure 6a, right panel).

We modeled both isomers of Cs-NAT-16 in the pressure range from 0 to 5 GPa; see Figure 5d for the $p-V$ diagram. Using the following formal equation

$$\text{Cs-NAT-16(isomer1)} \rightarrow \text{Cs-NAT-16(isomer2)} \quad (5)$$

we estimated the critical pressure p^* of the phase transition to be 1.0 ± 0.7 GPa. The uncertainty of 0.7 GPa is noticeably larger than the uncertainty values determined for the phase transitions of Na-NAT and Rb-NAT. In fact, the two linear fits for the enthalpies $H(p)$ of the two isomers of Cs-NAT are almost parallel in the range from 0.3 to 1.7 GPa. This may rationalize why experimentally two isomers were found to coexist. The estimated value of p^* agrees very well with the experimental range, 0.3−1.5 GPa (Table 4).[20] The quality of this result likely reflects the more realistic quality of the computational model because in Cs-NAT-16, eq 5, the number of water molecules per unit cell does not change. Therefore, different from the cases of Na-NAT and Rb-NAT, the corresponding entropy effects, omitted in the model, can be expected to cancel, at least to a significant part.

We did not directly follow the structure change under pressure of the phase transition of Cs-NAT, in view of the lack of temperature and entropy contributions. Instead, we modeled initial and final structures. The experimentally observed transition under pressure between the two isomers[20] is represented by a formal rotation by 90° of the (projected) arrangement of the Cs^+ ions and a formal rotation by 45° of the aqua ligands; these rotations take place around axes in the c direction, along the channels. Yet, the size of the Cs^+ ions makes a simple rotation inside the natrolite channels rather unlikely. In order to trace the rearrangement accompanying the phase transition, we assumed that under pressure the Cs^+ ions slip through the smaller pores in the [111] direction of the unit cell into the neighboring channels. This suggested mechanism is sketched in Figure 6a. To probe this scenario, we carried out a series of constrained structure optimizations at 1 GPa, the computationally estimated critical pressure. In these calculations, we fixed the relative positions of 16 Cs^+ ions in the unit cell while the volume of the unit cell as well as the positions of the other atoms in the unit cell were allowed to relax. Figure 6b shows the resulting energies profile, which features an energy barrier of only 45 kJ mol^{-1} per ion. This outcome seems to render the suggested path for the rearrangement of ions and water ligands between the channels more likely than the rearrangement of the ions and water molecules inside the channels.[20]

4. CONCLUSIONS

In the present study we modeled the monovalent cation-exchanged natrolites, Li-, Na-, K-, Rb-, and Cs-NAT, at ambient conditions. The optimized structures of Li- and Na-NAT agree well with the experimentally observed. For K-, Rb-, and Cs-NAT, experiments point to at least two isomers with different cation positions. The structures calculated for these natrolites resemble one of the experimental isomers. The distances from the cations to the closest water ligands in X-NAT fall into two groups, correlating roughly with the ionic radii of X^+: 2.11−2.40 Å for X = Li, Na and 2.93−3.22 Å for X = K, Rb, Cs. In agreement with these X−O distances, the interactions between alkali ions and water ligands in the natrolite framework were calculated to be stronger in Li- and Na-NAT than in K-, Rb-, and Cs-NAT. The stronger bonding between ions and water ligands in Li- and Na-NAT may be interpreted to yield more rigid cation−water chains, which, in turn, imply better defined positions of the cations in the zeolite framework.

Not unexpectedly, the natrolite framework is strained most when Na^+ ions are formally replaced by Rb^+ or Cs^+; the strain energies were calculated to be 80−100 kJ mol^{-1} per ion. The strain energy of K-NAT is notably lower, 45 kJ mol^{-1}. The cation-exchange energy, estimated relative to the hypothetical H-form of natrolite, shows that Na-NAT has the most stable structure among all alkali exchanged forms of natrolite.

The two DFT approaches used, PBE and PBE-D2 (with an empirical dispersion correction), showed quite similar results at ambient conditions, both agreeing well with experimental structures. However, the PBE-D2 method failed to reproduce the trend of the bulk modulus of superhydrated Na-NAT-32 and the $p-V$ diagram. Therefore, we examined the pressure-induced phenomena of natrolites, the superhydration of Na- and Rb-NAT, as well as the phase transformation of Cs-NAT using only the PBE functional.

The structures of Na-NAT with 16, 24, and 32 water molecules per unit cell and Rb-NAT with 16 and 32 water molecules per unit cell were explored at pressures up to 5 GPa. The critical pressure values of hydration estimated computationally overestimate somewhat the experimental ones, but the trends are reproduced quite well. To model the pressure-induced phase transformation in Cs-NAT, we calculated two isomers of Cs-NAT under pressure. The resulting critical pressure agrees even better with experiment than for Na- and Rb-NAT, probably because the phase transition occurs with a constant number of the water molecules present; hence, the corresponding entropy effects largely appear to cancel out. Using constrained structure optimizations, we proposed a novel path in configuration space between the two isomers of Cs-NAT. Along this path, the Cs^+ ions move through the small pores of natrolite to neighboring channels, thereby having to overcome only a rather low energy barrier, which was estimated to be 45 kJ mol^{-1} per Cs ion.

■ ASSOCIATED CONTENT

Supporting Information

Coordinates of the optimized structures, labels identifying symmetry-inequivalent O centers in the natrolite framework, data for $p-V$ diagrams for Na-, Rb-, and Cs-NAT, data for linear fits of the enthalpy $H(p)$ as a function of pressure p, and procedure of calculating the critical pressure p^* and estimating the corresponding uncertainties. This material is available free of charge via the Internet at http://pubs.acs.org.

■ AUTHOR INFORMATION

Corresponding Author

*E-mail: roesch@mytum.de.

Notes

The authors declare no competing financial interest.

■ ACKNOWLEDGMENTS

We thank Cheng-chau Chiu, Alexander Genest, and Sven Krüger for helpful discussions. Leibniz Rechenzentrum München provided a generous allotment of computational resources. T.V. would like to thank the Korean Ministry of

Science and Technology for funds associated with a Global Research Laboratory.

REFERENCES

(1) Breck, D. W. *Zeolite Molecular Sieves: Structure, Chemistry, And Use*; Krieger: Malabar, FL, 1984.
(2) Dyer, A. *An Introduction to Zeolite Molecular Sieves*; Wiley: Chichester, U.K., 1988.
(3) *Zeolites in Industrial Separation and Catalysis*; Kulprathipanja, S., Ed.; Wiley-VCH: Weinheim, Germany, 2010.
(4) Almutairi, S. M. T.; Mezari, B.; Filonenko, G. A.; Magusin, P. C. M. M.; Rigutto, M. S.; Pidko, E. A.; Hensen, E. J. M. *ChemCatChem* **2013**, *5*, 452.
(5) Eichler, U.; Brandle, M.; Sauer, J. *J. Phys. Chem. B* **1997**, *101*, 10035.
(6) Lee, Y.; Vogt, T.; Hriljac, J. A.; Parise, J. B.; Artioli, G. *J. Am. Chem. Soc.* **2002**, *124*, 5466.
(7) Lee, Y.; Hriljac, J. A.; Parise, J. B.; Vogt, T. *Am. Mineral.* **2005**, *90*, 252.
(8) Lee, Y.; Seoung, D.; Im, J. H.; Hwang, H. J.; Kim, T. H.; Liu, D.; Liu, Z.; Lee, S. Y.; Kao, C. C.; Vogt, T. *Angew. Chem., Int. Ed.* **2012**, *51*, 4848.
(9) Ross, M.; Flohr, M. J. K.; Ross, D. R. *Am. Mineral.* **1992**, *77*, 685.
(10) Alberti, A.; Pongiluppi, D.; Vezzalini, G. *Neues Jahrb. Mineral. Abh.* **1982**, *143*, 231.
(11) Grima, J. N.; Gatt, R.; Zammit, V.; Williams, J. J.; Evans, K. E.; Alderson, A.; Walton, R. I. *J. Appl. Phys.* **2007**, *101*, 086102.
(12) Love, A. E. H. *A treatise on the mathematical theory of elasticity*, 4th ed.; Dover: New York, 2011.
(13) Alderson, A.; Rasburn, J.; Ameer-Beg, S.; Mullarkey, P. G.; Perrie, W.; Evans, K. E. *Ind. Eng. Chem. Res.* **2000**, *39*, 654.
(14) Grima, J. N.; Jackson, R.; Alderson, A.; Evans, K. E. *Adv. Mater.* **2000**, *12*, 1912.
(15) White, C.; Ruiz-Salvador, A. R.; Lewis, D. W. *Angew. Chem., Int. Ed.* **2004**, *43*, 469.
(16) Lee, Y.; Hriljac, J. A.; Vogt, T.; Parise, J. B.; Artioli, G. *J. Am. Chem. Soc.* **2001**, *123*, 12732.
(17) Lee, Y.; Hriljac, J. A.; Vogt, T. *J. Phys. Chem. C* **2010**, *114*, 6922.
(18) Lee, Y.; Lee, Y.; Seoung, D. *Am. Mineral.* **2010**, *95*, 1636.
(19) Lee, Y.; Seoung, D.; Lee, Y. *Am. Mineral.* **2011**, *96*, 1718.
(20) Seoung, D.; Lee, Y.; Kao, C. C.; Vogt, T.; Lee, Y. *Chem. Eur. J.* **2013**, *19*, 10876.
(21) Baur, W. H. *J. Solid State Chem.* **1992**, *97*, 243.
(22) Baur, W. H.; Joswig, W.; Muller, G. *J. Solid State Chem.* **1996**, *121*, 12.
(23) Grima, J. N.; Farrugia, P. S.; Caruana, C.; Gatt, R.; Attard, D. *J. Mater. Sci.* **2008**, *43*, 5962.
(24) Kresse, G.; Hafner, J. *Phys. Rev. B* **1993**, *47*, 558.
(25) Kresse, G.; Hafner, J. *Phys. Rev. B* **1994**, *49*, 14251.
(26) Kresse, G.; Furthmüller, J. *Comput. Mater. Sci.* **1996**, *6*, 15.
(27) Kresse, G.; Furthmüller, J. *Phys. Rev. B* **1996**, *54*, 11169.
(28) Blöchl, P. E. *Phys. Rev. B* **1994**, *50*, 17953.
(29) Kresse, G.; Joubert, D. *Phys. Rev. B* **1999**, *59*, 1758.
(30) Perdew, J. P.; Burke, K.; Ernzerhof, M. *Phys. Rev. Lett.* **1996**, *77*, 3865.
(31) Perdew, J. P.; Burke, K.; Ernzerhof, M. *Phys. Rev. Lett.* **1997**, *78*, 1396.
(32) Wu, X.; Vargas, M. C.; Nayak, S.; Lotrich, V.; Scoles, G. *J. Chem. Phys.* **2001**, *115*, 8748.
(33) Grimme, S. *J. Comput. Chem.* **2006**, *27*, 1787.
(34) Poswal, H. K.; Sharma, S. M.; Sikka, S. K. *High Pressure Res.* **2010**, *30*, 198.
(35) Le Page, Y.; Saxe, P. *Phys. Rev. B* **2002**, *65*, 104104.
(36) Likhacheva, A. Y.; Veniaminov, S. A.; Paukshtis, E. A.; Belitsky, I. A. *Eur. J. Mineral.* **2006**, *18*, 345.
(37) Stuckenschmidt, E.; Kassner, D.; Joswig, W.; Baur, W. H. *Eur. J. Mineral.* **1992**, *4*, 1229.
(38) Shannon, R. *Acta Crystallogr., A* **1976**, *32*, 751.
(39) Smith, D. W. *J. Chem. Educ.* **1977**, *54*, 540.
(40) Mahler, J.; Persson, I. *Inorg. Chem.* **2012**, *51*, 425.
(41) *CRC Handbook of Chemistry and Physics*, 84th ed.; Lide, D. R., Ed.; CRC Press: Boca Raton, FL, 2003.
(42) Baur, W. H.; Kassner, D.; Kim, C. H.; Sieber, N. H. W. *Eur. J. Mineral.* **1990**, *2*, 761.
(43) Angel, R. J. In *High-Temperature and High-Pressure Crystal Chemistry*; Hazen, R. M., Downs, R. T., Eds.; The Mineralogical Society of America: Washington, DC, 2000; Vol. *41*, pp 35−58.